Characteristics of static shift in 3-D MT inversion

Tae Jong Lee*, Toshihiro Uchida**, Yutaka Sasaki*** and Yoonho Song*

* : Korea Institute of Geoscience and Mineral Resources, Korea: megi@kigam.re.kr, song@kigam.re.kr

** : Institute of Geo-Resources and Environment, AIST, Japan: uchida-toshihiro@aist.go.jp

*** : Kyushu Univ., Japan: sasaki@mine.kyushu-u.ac.jp

1. Introduction

Galvanic distortion (Groom and Bailey, 1989) is usually caused by the presence of charges on local, small scale, shallow, lateral inhomogenities. The charge built up at the interfaces of small scale near-surface inhomogenities compared to the penetration depth of the EM field produces frequency-independent distortion of electric fields (see, for example, deGroot-Hedlin, 1991). The distortion affects on the electric field only, so that it appears as parallel shifts in MT sounding curves when plotted in log (apparent resistivity) vs. log (period) scale. The phenomenon is called "static shift" and often ranges over three orders of magnitude, which is frequently observed in resistive crystalline terrains (Kurtz et al., 1993). Because the entire data is affected by small-scale shallow feature, the static shift will lead severe distortion in inverted resistivity structures. Removing static shift is a critical problem and will vastly improve interpretation of MT data.

Various methods for static shift removal have been developed as is summarized in Sternberg et al. (1988). They can be loosely divided into three categories: 1) spatial filtering by closely spaced MT sites, i.e., Electro-Magnetic Array Profiling (EMAP: Torres-Verdin, 1991, Bostick, 1986), 2) theoretical calculations of the static shift from buried near-surface inhomogeneities or surface topographic effects (Wannamaker et al., 1984), 3) use of auxiliary data from known geology or independent measurement such as TEM coincident sounding (Sternberg et al., 1988). All of these techniques have successively applied to static shift compensation. They, however, may be prohibitively costly to acquire the extra-data at the necessary number of sites particularly in large regional surveys.

Alternative method, which does not require additional information, was suggested by DeGroot-Hedlin (1991). It solves simultaneously for static shift parameters as well as block

resistivities as inversion parameters. This method assumes that total sum of static shift parameters, for all sites and modes, is close to zero. Sasaki (2001) applied the static shift parameterization to 3-D MT inversion using finite difference forward calculation.

Based on Sasaki's code, in this paper, some modifications are made to the code and characteristics of static shift are considered using a numerical model with varying static shift contents in the data. The modifications are mainly in two categories; one is to add weighting based on the errors in the data, and the other is to add a routine for searching best trade-off parameter for static shift. At first in this paper, we will discuss about a little detail about static shifts, and the theory of smooth inversion scheme will be followed. And then numerical examples will be demonstrated.

2. Parameterization of static shift

For frequencies that are sufficiently low, the size of the inhomogeneity is small with respect to the wavelength within the inhomogeneity, it can be shown that the magnetic field is unaffected by the buildup of boundary charges (Wannamaker et al., 1984) and that the secondary electric field is independent of frequency (deGroot-Hedlin, 1991). The effect of near surface inhomogeneities is thus to scale the electric field by a multiplicative factor:

$$\rho_a^{obs} = k\left|\frac{E^{obs}}{H}\right| = k\left|\frac{\alpha E'}{H}\right| = \alpha\rho_a' \tag{1}$$

where superscript 'obs' stands for 'observed' and ρ_a' is undistorted apparent resistivity, which represents the real structure. At high frequencies, however, when the skin depth is less than the scale size of the inhomogeneity, the secondary electric field is no longer frequency independent.

Taking logarithm in both side of equation (1),

$$\log(\rho_a^{obs}) = \log(\rho_a') + g \tag{2}$$

This means that the static shift appears as up/down shift of MT sounding curves in log-log plot.

By the analogy of equation (2), the MT data in the presence of static shift s can be described as

$$\mathbf{d} = \mathbf{F(m)} + \mathbf{Gs}, \tag{3}$$

where d is the calculated data, F is a non-linear function describing forward MT problem for a given model m , and G is a matrix relating the static shift values to the data. The rows of G

corresponding to phase or tipper data, which will not be affected by static shift, are identically zero: and the rows corresponding to the apparent resistivities have unity at the appropriate locations. The objective function to be minimized is defined as

$$U = \left\| \mathbf{W}\left[\Delta\mathbf{d} - \mathbf{A}\Delta\mathbf{m}^{(k)} - \mathbf{Gs} \right] \right\|^2 + \lambda^2 \left(\left\| \mathbf{Cm}^{(k+1)} \right\| + \alpha^2 \left\| \Delta\mathbf{m} \right\| + \beta^2 \left\| \mathbf{s} \right\|^2 \right) \qquad (4)$$

where W is weights related to the observation errors, A is the Jacobian matrix, C is a roughening matrix, and λ and β are tradeoff parameters for roughness and static shift, respectively. The first term in equation (2) represents data misfit, the second represents the constraints to control the smoothness of the solution, the term with α represents the Marquadt constraint, and the last constraints on the static shift. Here, it is applied a constraint that the static shift s statistically has a Gaussian distribution. Starting from the initial model $\mathbf{m}_0$, iteration is continued until desired level of misfit is achieved. At each iterations, another loop for searching for the best tradeoff parameter λ and β is added to find the best model and static shift parameters based on the rms misfit. The two parameters are closely related to each other as in equation (4). The parameter λ controls the smoothness of the inverted model as well as the amount of static shift in the form of $\lambda \times \beta$.

The forward computation F(m) for a given model m is done by staggered grid finite difference method (FDM) (Sasaki, 1999).

3. Numerical examples

Figure 1 shows a model configuration for the test model, which has a conductor of 10 ohm-m and a resistor of 1000 ohm-m in a homogeneous background of 100 ohm-m. The two bodies have the same size of $1.0 \times 1.5 \times 1.0$ km. Sixty three measurement points with 500 m spacing in x and y directions are located on the surface. Six frequencies from 0.3 Hz to 100 Hz are used. At each measuring point, apparent resistivity and phase for TE (x-y) and TM (y-x) mode are gathered, which makes 1512 known data. 3% of random noise is added to both the log-resistivity and phase in radian. Then random Gaussian static shift of zero mean with standard

deviation of 0.3. In this case, static shift ranges from -0.75 to 0.64, which correspond to 0.47 to 1.90 times in apparent resistivity. For the inversion, the earth is discretized into 891 ($11\times9\times9$) blocks as shown with bold lines in Figure 1. The starting model for the inversion is 100 ohm-m half-space.

Figure 2 shows the block resistivities from the two inversion schemes, and Figure 3 shows estimated static shift parameters for the two modes at each site. As can be seen in Figure 3, the inversion estimates static shift parameters quite well and the block resistivity from the scheme separates the deep seated

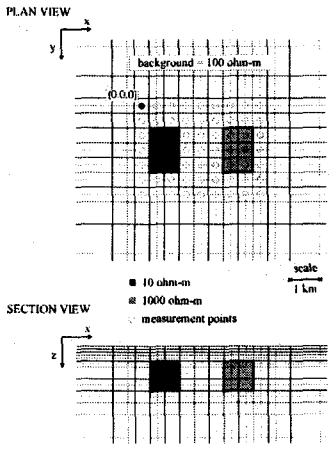

Fig. 1. A plan view and section view for the test model in this study. Two anomalous bodies with the same size of 1 km * 1.5 km * 1 km are located in the same depth of 1 km in 100 ohm-m half-space. The resistivity of a conductor is 10 ohm-m and the other body have 1000 ohm-m, respectively.

conductor as well as the resistor quite well as can be seen in Figure 2(a). Note in Figure 2(a) that all the surface blocks show almost homogeneous of 100 ohm-m. Physically, static shift mainly occurs by the inhomogeneities on the surface. In that case the phase also should be changed as frequency getting high. At high frequencies, when the skin depth is less than the size of the inhomogeneity, the static effect is no longer frequency independent. In this study, however, the static shift are given to the apparent resistivity only, which can be occurred when there exists surface inhomogeneities with very small size, the dimension is smaller than the

skin depth at highest frequency measured.

Conventional inversion result in Figure 2(b) shows very complex surface inhomogeneities. It seems that the inversion tried to generate static shifts by modifying the resistivity of surface blocks. And by this, the inversion reconstructed the deeper structures conductor and the resistor to some extent.

Figure 4 compares the simulated apparent resistivity and phase data with the observed ones for the result shown in Figure 2(b). One can find typical static shift effect at low frequencies from both of the figure. The calculated and observed apparent resistivity shows parallel up/down movement independent of the frequency, while the phase shows very good match. Though the inversion tried to remove the static shift by changing the resistivity of the surface block, the static shift still remains. Note that the inversion fails to fit the phase data at high frequencies above 30 Hz. Changing the block resistivity on the surface causes the distortion of phase at high frequencies.

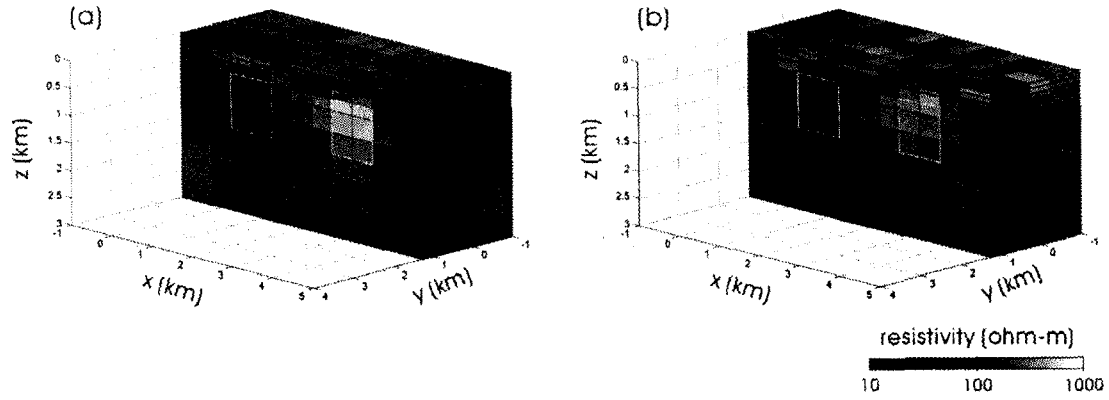

Fig. 2. Reconstructed images for the model shown in figure 2 with random Gaussian static shifts with its standard deviation of 0.3 are added. The inversion with static shift parameters (a) shows reasonable estimation of block resistivities. But when the static shift parameters are not allowed (b), the inversion tries to generate static shift by modifying the resistivity of surface blocks.

4. Concluding remarks

Galvanic distortion by small-scale shallow feature will lead severe distortion in inverted resistivity structures. In conventional MT survey we usually do not have any additional information about static shift. Simultaneous inversion of block resistivity and static shift

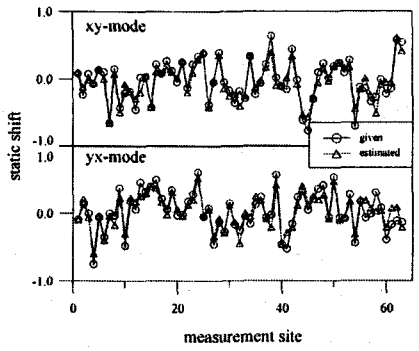

Fig. 3. Estimated static shift parameters for the dataset1, 3 % random Gaussian static shifts are added. Note that the estimated static shift closely approaches to the given values

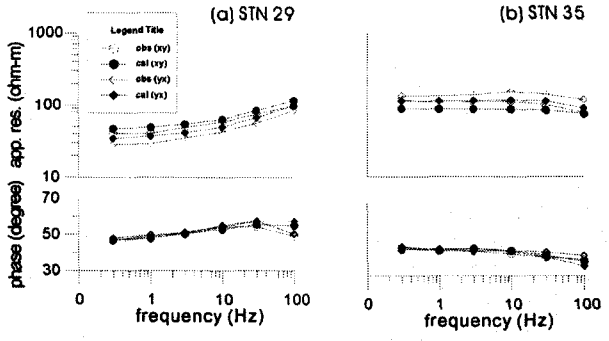

Fig. 4. The comparison between observed and calculated responses at stations 29 and 35 for the inversion driven the result in Figure 5(b). The conventional inversion tried to generate the static shift by changing the resistivity of the surface blocks. It however fails to fit the phase data at high frequencies above 30 Hz in both stations

parameters is a good alternative to deal with the problem. In such case the determination of appropriate weighting for static shift parameter and the smoothness constraint is important.
In this study, characteristics of static shift in 3-D MT inversion are discussed using a theoretical data with random Gaussian static shift. Simultaneous searching for appropriate weighting for both static shift parameters and the model smoothness based on the rms misfits at each iteration, showed quite reasonable estimate of the amount of the static shift components contained in the data. The 3-D inversion with static shift parameterization efficiently separates the Gaussian static shifts in the data, and even when the static shift does not obey the Gaussian distribution (not shown). Allowing the degree of freedom by the static shift parameters, the inversion could get more accurate block resistivities as well as given static shifts.

When the inversion does not consider the static shift as inversion parameters, the block resistivities on the surface are modified considerably to match possible static shift. By those mechanisms, the conventional 3-D MT inversion can reconstruct the resistivity structures in deeper parts, when the static shift is not so strong. As frequency increased, however, the galvanic distortion is not frequency independent any more, and thus the conventional inversion failed to fit the apparent resistivity and phase, especially when strong static shift is added.

Acknowledgments

The authors are grateful to Dr. Yasuo Ogawa for his helpful suggestion during the work and to JISTEC for financial support. TJL was partly supported by KORP (Korea Research Council of Public Science & Technology) funding to KIGAM (Korea Institute of Geoscience and Mineral Resources). TJL and TU used a computer system at the Tsukuba Advanced Computer Center, AIST.

References

Bostick, F. X., 1986, Electromagnetic Array Profiling (EMAP): 56th Ann. Mtg., Soc. Expl. Geophys., Expanded Abstracts, 60-61.

deGroot-Hedlin, C., 1991, Removal of static shift in two dimensions by regularization inversion: Geophysics, 56, 2102-2106.

Groom, R. W. and Bailey, R. C., 1989, Decomposition of magnetotelluric impedance tensors in the presence of local three-dimensional galvanic distortion: J. of Geophys. Res., 94, 1913-1925.

Kurtz, R. D., Craben, J. A., Niblett, E. R., and Stevens, R. A., 1993, The conductivity of the crust and mantle beneath the Kapuskasing Uplift - electrical anisotropy in the upper mantle: Geophys. J. Int., 113, 483-498.

Sasaki, Y., 2001, Three-dimensional inversion of static-shifted magnetotelluric data: Proc. 5th SEGJ International Symposium, 185-190.

Sternberg, B. K., Washburne, J. C., and Pellerin, L., 1988, Correction for the static shift in magnetotellurics using transient electromagnetic soundings: Geophysics, 53, 1459-1468.

Torres-Verdin, C., 1991, Continuous profiling of Magnetotelluric Fields: Ph. D thesis, Univ. of California Berkeley.

Wannamaker, P. E., Hohmann, G. W., and Ward, S. H., 1984, Magnetotelluric responses of three-dimensional bodies in layered earths: Geophysics, 49, 1517-153